JACS
JOURNAL OF THE AMERICAN CHEMICAL SOCIETY

Article

pubs.acs.org/JACS

Framework-Topology-Dependent Catalytic Activity of Zirconium-Based (Porphinato)zinc(II) MOFs

Pravas Deria,[*,†,§,#] Diego A. Gómez-Gualdrón,[‡,#,⊥] Idan Hod,[†] Randall Q. Snurr,[*,‡] Joseph T. Hupp,[*,†] and Omar K. Farha[*,†,∥]

[†]Department of Chemistry, and [‡]Department of Chemical and Biological Engineering, Northwestern University, 2145 Sheridan Road, Evanston, Illinois 60208, United States

[§]Department of Chemistry, Southern Illinois University, 1245 Lincoln Drive, Carbondale, Illinois 62901, United States

[∥]Department of Chemistry, Faculty of Science, King Abdulaziz University, Jeddah 21589, Saudi Arabia

Supporting Information

ABSTRACT: Catalytic activity for acyl transfer from *N*-acetylimidazole (NAI) to different pyridylcarbinol (PC) regioisomers (2-PC, 3-PC, and 4-PC) is demonstrated for a set of topologically diverse, zirconium-based (porphinato)zinc metal−organic frameworks (MOFs). The MOFs studied are PCN-222, MOF-525, and NU-902, which are based on the ***csq***, ***ftw***, and ***scu*** topologies, respectively. The experimentally obtained reaction kinetics are discussed in light of molecular modeling results. The catalytic activity is shown to vary across the series of MOFs due to the different extent to which each topology facilitates reactant preconcentration and alignment of PC and NAI via coordination to framework porphyrin sites (orientation effects). Trends of experimental initial reaction rates with MOF topology and PC regioisomer are consistent with preconcentration effects, which depend on the number of porphyrin sites per volume of MOF, as well as with orientation effects, which depend on the number of porphyrin pairs per volume of MOF that bind PC and NAI in such a way that they are primed to form the required transition state. The present work shows how the proper alignment of catalytic linkers can enhance reaction rates in MOFs.

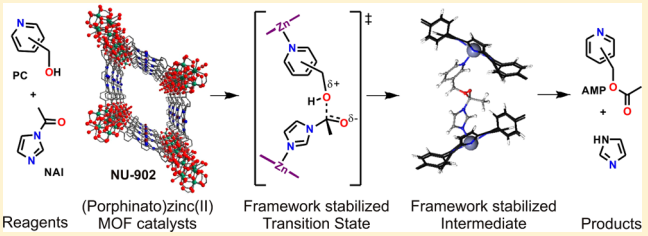

INTRODUCTION

Metal−organic frameworks (MOFs) are porous materials formed by metal ions or metal oxide clusters connected by multitopic organic linkers.[1] The modular nature of MOFs allows, in principle, for virtually unlimited combinations of inorganic and organic building units to form chemically diverse, crystalline materials based on different network topologies.[2] Indeed, the enormous design flexibility of pore geometries and chemical functionalities, along with high specific internal surface areas, makes MOFs highly desirable for catalysis.[3] While high surface areas can provide access to a large number of well-defined catalytic sites within the framework structure, the geometric characteristics of the MOF pores can be tuned and exploited to achieve high selectivity.[3a,c,d,4]

Numerous examples of MOF catalysts involve the immobilization of well-established homogeneous catalysts as part of the MOF structure, resulting in well-defined catalytic sites but with improved stability (due to elimination of some deactivation pathways) as well as recyclability.[5] However, it is rare to find examples where the catalytic activity stems from a unique spatial distribution of potential binding/active sites that is achievable only within a specific MOF structure. Because the spatial orientation of MOF building blocks is a function of topology, the topological diversity of MOFs can be exploited to alter the position and orientation of MOF catalytic sites, which can be located at the nodes and/or linkers.[6] Note that in applications such as gas storage, MOF topology has already been shown to affect performance.[7] In chemical catalysis, concerted binding[8] of reactants to facilitate the formation of an energetically favorable transition state or intermediate through the involvement of suitably oriented "neighboring active sites" is often the means by which rates are accelerated. In principle, such effects should also be achievable with appropriately designed MOFs, where the needed design elements are likely to include selection of an appropriate MOF topology.

Zr-based MOFs are particularly attractive due to their robust structures,[5b,9] where strong Zr^{IV}−carboxylate coordination bonds have facilitated the synthesis of, for instance, water-stable MOFs with ultrahigh surface areas.[10] The stability of Zr-based MOFs and the possibility of incorporating different chemical functionalities via postsynthesis approaches such as solvent-assisted linker exchange (SALE) and solvent-assisted ligand incorporation (SALI) have propelled the study of these materials for a wide range of applications.[5a,b,10,11] Recently, microporous and mesoporous Zr-based MOFs with metalloporphyrin linkers have been reported as highly stable, catalytically active systems.[5a,b,11e,l,12] An intriguing subclass of

Received: August 31, 2016
Published: October 21, 2016

DOI: 10.1021/jacs.6b09113
J. Am. Chem. Soc. 2016, 138, 14449−14457

Zr-based porphyrin MOFs are those featuring as linkers the tetra-anionic form (deprotonated form) of H_4TCPP (tetrakis(4-carboxyphenyl)porphyrin). The functionalized porphyrins can assemble into a variety of network topologies (Figure 1) including ***csq*** (PCN-222/MOF-545[5a,11c]), ***ftw*** (MOF-525[11c]), ***shp*** (PCN-223[11e]), and ***sqc*** (PCN-225[5b]).

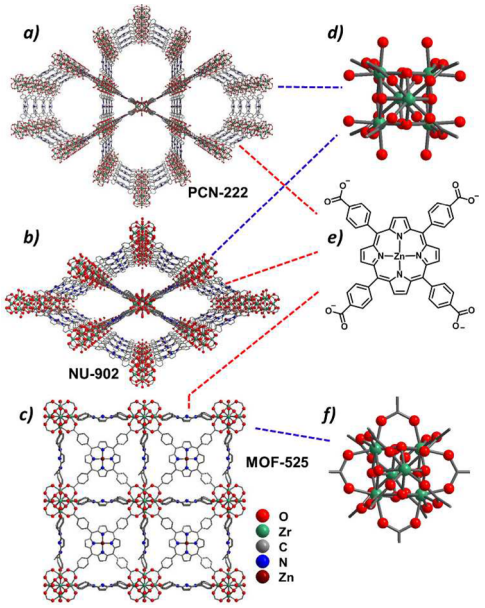

Figure 1. Molecular structures of (a) PCN-222, (b) NU-902, and (c) MOF-525. Corresponding Zr_6-oxo nodes (d, f) and the linker (e; carboxylate form of Zn−TCPP) are presented on the right.

We hypothesized that in the above series of chemically similar, but topologically different, MOFs, catalytic activity occurring within the MOF pores could be influenced by topology if the reaction requires orientation-specific, concerted binding of reactants by the metalated porphyrin centers. As a proof of concept, we evaluated the catalytic activity of the Zn(II)-metalated versions of two porphyrin-containing zirconium MOFs, PCN-222 (***csq***) and MOF-525 (***ftw***), as well as the new MOF NU-902 (***scu***). The putative MOF-topologically dependent reactions examined were the Lewis-acid-catalyzed transfer of an acyl group[13] from *N*-acetylimidazol (NAI) to 2-, 3-, or 4-pyridylcarbinol (PC). We also describe the synthesis and characterization of NU-902.

EXPERIMENTAL SECTION

Materials. Solvents including acetone (Macron, 98%), *N*,*N*′-dimethylformamide (DMF) (Macron, 99.8%), dichloromethane (Macron, 99.0%), *N*,*N*′-diethylformamide (DEF) (TCI America), deuterated dimethyl sulfoxide (d_6-DMSO), and sulfuric acid (D_2SO_4) (Cambridge Isotopes, 96−98% solution in D_2O) were used as received without further purification. The pyridylcarbinols (2-PC, 3-PC, and 4-PC), *N*-acetylimidazole (NAI), biphenyl, zirconyl chloride octahydrate, anhydrous zinc chloride, and benzoic acid were purchased from Sigma-Aldrich and used as received. Tetrakis(4-carboxyphenyl)porphyrin (H_4TCPP) was purchased from Frontier Scientific as dry powder and was directly used as received.

Instrumentation. Powder X-ray diffraction (PXRD) patterns were recorded on a Rigaku ATXG diffractometer equipped with an 18 kW Cu rotating anode, MLO monochromator, and a high-count-rate scintillation detector (measurements made over a range of $1.5° < 2\theta < 30°$ in 0.05° step width with a 2 deg/min scanning speed). ^{1}H NMR spectra were recorded on an Agilent 400 MHz instrument after digesting the samples in 10% D_2SO_4/DMSO-d_6. Diffuse reflectance Fourier transformed infrared spectra (DRIFTS) were recorded on a Nicolet 7600 FTIR spectrometer equipped with an MCT detector. The spectra were collected in a KBr mixture. Scanning electron microscopy (SEM) images and energy dispersive X-ray spectroscopy (EDS) were recorded on a Hitachi SU8030 SEM. Nitrogen isotherms were measured on a Micromeritics TriStar II 3020 at 77 K; for BET area calculations, we ensured that the consistency criteria proposed by Rouquerol et al.[14] were satisfied as discussed recently for MOFs.[15]

Synthesis. *i. Synthesis of PCN-222 and MOF-525.* Microcrystalline PCN-222 (also known as MOF-545) was prepared solvothermally in the presence of $ZnCl_2$ following a published protocol.[5a] The as-synthesized PCN-222 material featuring (porphinato)zinc(II) and four benzoates per node was not treated with HCl/DMF for benzoate removal;[5a,11b] instead it was sequentially washed with DMF and acetone (4 × 10 mL each for 100 mg sample) prior to thermal activation at 120 °C for 12 h. MOF-525 was also prepared following a procedure in the literature.[16] The as-synthesized MOF-525 featured a free-base porphyrin core,[11c,16] which was subsequently metalated with Zn(II) (vide infra). After the solvent was exchanged for acetone, the as-synthesized material was thermally dried (see Figure SI-2 for the PXRD pattern).

ii. Synthesis of NU-902. Zirconyl chloride octahydrate (11 mg; 0.033 mmol) and benzoic acid (750 mg; 6.113 mmol) were placed in a 6-dram vial (VWR) and dissolved in 10 mL of DMF via sonication (10 min). The resulting solution was incubated in an oven at 80 °C for 45 min and then cooled to room temperature, at which point H_4TCPP (25 mg; 0.031 mmol) was added. The mixture was sonicated (10 min) forming a clear solution, which was heated in an oven at 90 °C for 2 d. After being cooled to room temperature and removing the mother liquor, the resulting microcrystalline powder was centrifuged and washed with fresh DMF five times over the course of 3 days. The solid sample was exchanged and washed with acetone (4 × 15 mL) and dried in a vacuum (∼100 Torr) for 30 min at 50 °C to yield ∼20 mg of activated MOF.

For the activation involving the removal of ligated benzoates, 0.5 mL of 8 M HCl (aq) was added to a portion of isolated as-synthesized material solid (∼75 mg) suspended in DMF (10 mL in total), and the resulting suspension was heated in a 100 °C oven for 18−24 h (see Figures SI-3−5). The suspension was then cooled to room temperature, centrifuged (5 min, 7000 rpm), and washed (3 × 12 mL) with fresh DMF. The residual solid was soaked (overnight), washed with acetone (4 × 15 mL), and finally dried in a vacuum (∼100 Torr) for 30 min at 50 °C to yield ∼50 mg of activated MOF.

iii. Postsynthesis Metalation of NU-902 and MOF-525. The Zn(II)-metalated MOF samples were prepared according to published protocol.[11c] Briefly, a portion of benzoate removed NU-902 or MOF-525 was added to a zinc chloride solution (10 mL of 0.062 M in DMF) and was heated at 100 °C for 18 h with occasional swirling. The microcrystalline powder was collected by centrifugation (5 min, 7000 rpm) and washed sequentially with DMF (5 × 10 mL) and acetone (5 × 10 mL). The solvent was finally dried in a vacuum (∼100 Torr) at 60 °C for 24 h. The extent of metalation was checked via analysis of Q-band signatures (Figure SI-6) corresponding to the low-energy electronic transition spectra for the porphyrinic macrocycles on the MOF samples decomposed in a 0.1 M NaOH solution. The absorption spectroscopic data were further corroborated by SEM-EDS data (see Figure SI-7). The metalation process was repeated in cases where the free-base signature was detected in the MOF samples.

Catalysis. Catalytic reactions were carried out under conditions identical to those published elsewhere.[12b] For acyl transfer reactions, stock solutions of *N*-acetylimidazole (60 mM); 2-, 3-, or 4-PC (90 mM); and biphenyl (25 mM) were made in HPLC grade acetonitrile solvent. Portions of biphenyl and PC stock (1 mL each) and MOF catalyst (10 mol % with respect to Zn−TCPP) were taken into an 8-dram screw-cap vial and diluted with 7 mL of acetonitrile. The mixture was stirred for 5 min before the addition of NAI stock solution (1 mL), after which the vial was placed in a heating block at 60 °C, with the block being mounted on a shaker (Thermolyne Maxi-Mix III). Aliquots (0.2 mL) were periodically collected and passed through a Celite 545

DOI: 10.1021/jacs.6b09113
J. Am. Chem. Soc. 2016, 138, 14449−14457

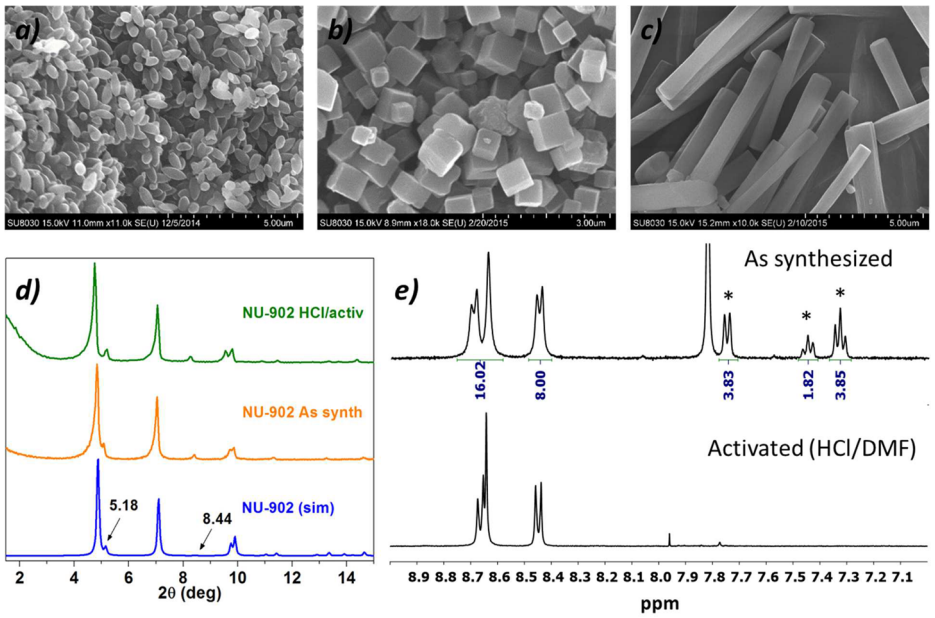

Figure 2. Representative SEM pictures of (a) NU-902, (b) MOF-525, and (c) PCN-222. (d) PXRD patterns and (e) partial ^{1}H NMR spectra of as-synthesized and HCl-activated NU-902; NMR spectra were taken after decomposing the material in 10% D_2SO_4/DMSO-d_6 mixture; ^{1}H signals for the benzoate ligands are denoted by "*".

Scheme 1. Lewis Acid-Catalyzed Acyl Transfer Reaction between Pyridylcarbinol (PC) and *N*-Acylimidazole (NAI) in a Zirconium-Based (Porphinato)zinc(II) MOF

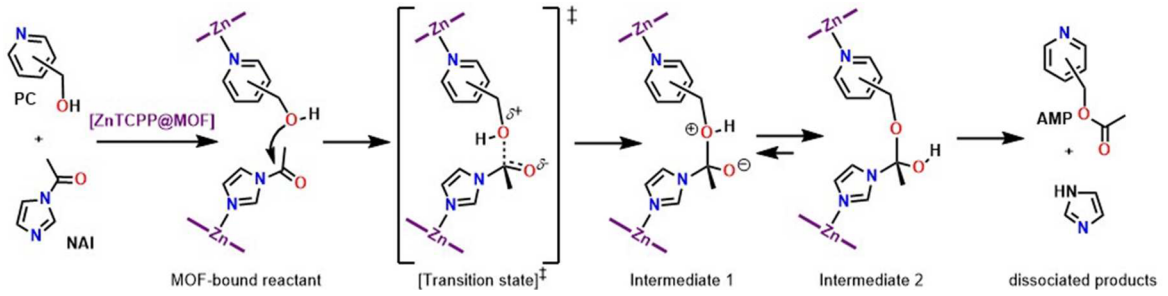

plug (0.5 cm × 3 cm) and eluted with diethyl ether (4 mL). Gas chromatography was performed on the samples using the following procedure and conditions: initial temperature = 70 °C, initial time = 2 min, ramp = 10 °C/min, final temperature = 200 °C, final time = 5 min.

RESULTS

Synthesis and Characterization of MOFs. Solvothermal reactions of $ZrOCl_2 \cdot 8H_2O$, tetrakis[4-carboxyphenyl]porphyrin (TCPP), and benzoic acid in DMF yielded a crystalline material with particles size ~300 nm, whose size was not suitable for single-crystal X-ray analysis. The structure was modeled in silico on the basis of the PXRD, FTIR, and ^{1}H NMR spectroscopy data. The initial model structure was taken from a previously reported database of 204 zirconium-based MOFs created in silico.[7] The modeling suggests that the framework possesses the (4, 8)-connected ***scu*** topology, with nodes identical to the 8-connected hexa-zirconium-oxo, -hydroxo cluster found in the ***csq*** topology.[7] Unlike the 12-connected zirconium SBUs (SBU = secondary building unit) in the ***ftw*** topology, the 8-connected zirconium SBU in the ***scu*** net leaves four positions for benzoate coordination. The benzoate ligands can be removed via HCl-activation of the intact MOF and, if desired, reattached using methods such as SALI.[5a,11b,17] Indeed, the ^{1}H NMR spectroscopy data for the as-synthesized sample (digested in D_2SO_4, Figure S-3) suggest the presence of four benzoates, which were successfully removed upon HCl/DMF treatment (or HCl activation) to expose four aqua and four hydroxo ligands at the node termini, pointing toward the channel.[11b,17] The nitrogen adsorption isotherm of the dried, as-synthesized NU-902 is type I (Figure SI-4a), and after activation a small step, indicative of mesopore formation, was observed. We ascribe this step to removal of a small fraction of the TCPP linker leading to defect sites with larger pores, consistent with the pore size distributions in Figure SI-4b. Brunauer–Emmett–Teller (BET) analysis of the isotherms (Figure SI-4) indicates an increase in BET area from 1580 to 2150 $m^2\ g^{-1}$ upon benzoate removal (HCl activation). Nitrogen adsorption data indicate that the HCl-activated samples feature a pore diameter of 12 Å. To find the optimal activation conditions, we treated identical amounts (75 mg) of as-synthesized MOF with varying amounts (0.2–1.0 mL) of 8 M HCl (aq) in DMF (10 mL). The resulting materials exhibited identical nitrogen isotherms (see Figure SI-4), implying that complete activation is achieved even with only 0.2 mL of HCl. DRIFTS measurements (see Figure SI-5) reveal the signature peaks, between 3600 and 3700 cm^{-1}, corresponding to terminal and bridging O–H stretches. For the as-synthesized samples, featuring four benzoates per zirconium node, a single peak at 3669 cm^{-1} consistent with the bridging μ_3-

DOI: 10.1021/jacs.6b09113
J. Am. Chem. Soc. 2016, 138, 14449–14457

OH groups is observed.[6a,17a,b,d] Upon activation with HCl/DMF, however, a peak appears at 3674 cm^{-1}, which we attribute to terminal −OH groups consistent with the removal of benzoates leaving aqua and hydroxyl ligands at the termini. Also, a shoulder at 3669 cm^{-1} appears corresponding to the bridging μ_3-OH groups similar to that reported for related MOFs.[17a,b,d,18] Increasing the HCl concentration during the activation process did not change the DRIFTS signature or the relative peak intensities, including that observed at 3325 cm^{-1} for the pyrrolic N−H (Figure SI-5). On the basis of these results, together with previous findings, the parent MOF consists of octahedral $[Zr_6(\mu_3\text{-}O)_4(\mu_3\text{-}OH)_4(\text{-}OH)_4(\text{-}OH_2)_4]^{8+}$ nodes and has the formula $Zr_6(\mu_3\text{-}O)_4(\mu_3\text{-}OH)_4(\text{-}OH)_4(\text{-}OH_2)_4(TCPP)_2$.

Powder X-ray diffraction (PXRD) measurements (Figure 2d; Figure SI-1) on the synthesized NU-902 materials are in excellent agreement with the simulated PXRD pattern obtained for the modeled structure. Note the presence of low-intensity peaks at 2θ values of 5.2° and 8.4° (Figure 2d, denoted with arrows) stemming from (100) and (120) planes, respectively. These peaks do not appear in the closely related MOF PCN-223,[11e] which is based on the ***shp*** topology and characterized by triangular channels.[19]

Catalytic Activity. As noted above, we took advantage of the Lewis acidity of MOF-based (porphinato)zinc(II) units to catalyze acyl-transfer between *N*-acetylimidazole (NAI) and pyridylcarbinol (PC) (Scheme 1).[13] The acyl-transfer reaction can, in principle, be facilitated (catalyzed) by a porphryinic MOF[5c] in any or all of three ways: (i) Lewis-acid activation through the coordination of NAI to the axial site of the Zn−TCPP to stabilize the negative charge on the acyl oxygen, (ii) preconcentration, wherein the coordination of reactants to Zn−TCPP sites within the MOF pores boosts the reaction-relevant local concentration of the acyl-group donor and/or acceptor (independently of changes in activation energies), and (iii) orientation optimization, where not only do reactants bind to Zn−TCCP sites, but they do so in a complementary fashion. In other words, the pyridine and imidazole components of PC and NAI, respectively, bind to neighboring Zn−TCPPs in such a way that the positions and orientations of the hydroxyl and carbonyl moieties of PC and NAI, respectively, facilitate the formation of a suitable transition state.[12b,18b]

The acyl transfer reactions produce acetoxymethylpyridines (AMP), whose solution concentrations as a function of time are shown in Figure 3 and Figure SI-8. Figure 3 illustrates the formation of 3-AMP in NU-902 (***scu***), PCN-222 (***csq***), and MOF-545 (***ftw***), as well as the formation of 4-AMP and 2-AMP in NU-902 (***scu***). In all cases, the kinetic analysis of AMP formation was aided by a monoexponential fitting of the experimental data, with the extracted (initial) reaction rates summarized in Table 1. Inspection of the reaction rate for 3-PC clearly shows the beneficial role of the MOF, which increases the rate by 2−3 orders of magnitude with respect to the uncatalyzed solution-phase reaction, and 1−2 orders of magnitude with respect to the reaction in the presence of an unsupported (solution phase) porphyrinic catalyst. Closer inspection of 3-PC reaction rates reveals that the extent of reaction enhancement depends significantly on the identity of the MOF. The highest initial rate for 3-PC with MOF-525 is about double that of the reported (porphinato)zinc(II)-based MOF.[12b,20]

Inspection of all kinetic data presented in Table 1 shows that the initial reaction rate depends both on the MOF topology as well as on the PC regioisomer. Under the reasonable assumption that Lewis-acid activation of the NAI reactants is

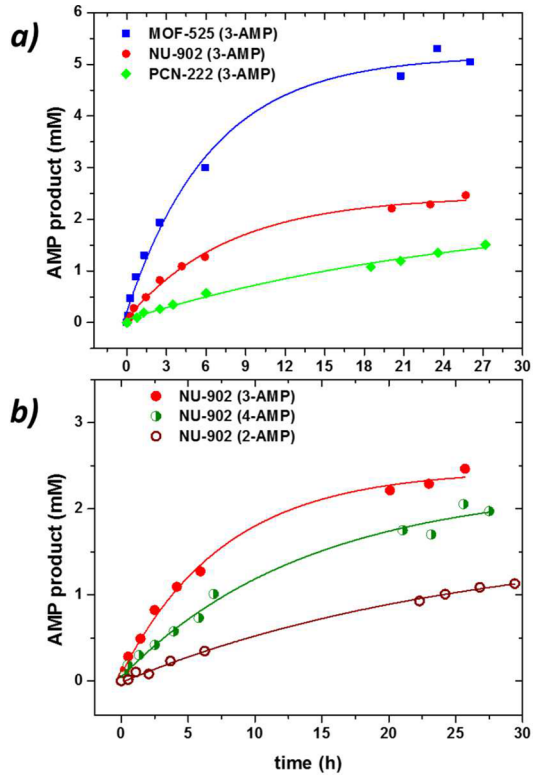

Figure 3. Kinetics of catalyzed acyl transfer reaction as a function of MOF topology and regiochemistry of the substrate. Plot of product concentrations versus time, showing the (a) rate of formation of 3-acetoxymethylpyridine (AMP) from *N*-acetylimidazole (NAI) and pyridylcarbinols (PC) in each of three MOFs and the (b) rate of formation of various regioisomers of AMPs in NU-902. [All MOFs feature only Zn−$TCPP^{4-}$ as linkers. The experiments were carried out under identical conditions (see Experimental Section). Solid lines represent fits of experimental data to single-exponentials.]

Table 1. Comparison of Initial Rate (mM/h) of the Acyl Transfer Reaction with Various PC Regioisomers for Heterogeneous (Porphyrinato)zinc(II) Catalysts As a Function of MOF Topology

MOF (topology)	2PC[a]	3PC[a]	4PC[a]
NU-902 (***scu***)	0.065	0.302	0.158
MOF-525 (***ftw***)	0.137	0.760	0.612
PCN-222 (***csq***)	0.036	0.079	0.083
TPP-Zn[b]		0.004	
uncatalyzed[b]		0.002	

[a]6 mM NAI, 9 mM PC, and 10 mol % Zn−TCPP within MOF samples at 60 °C; rates are reported in units of mM/h; see Experimental Section for detailed experimental conditions. [b]Homogeneous reaction under identical condition with or without Zn−TPP (Zn−TPP = 5,10,15,20-tetraphenyleporphinatozinc(II); see ref 12b).

similar for all Zn−TCPP sites in the three studied MOFs, then differences in reaction rate for the various regioisomer/MOF combinations must stem from the different degrees of preconcentration and complementary coordination of NAI and PC reactants arising from the different topologies (and thus spatial arrangements of Zn−TCCP linkers) of the three studied MOFs. The degree of preconcentration clearly is a function, at least in part, of the number of accessible Zn−TCPP sites within a given volume of MOF. Furthermore, given identical linkers and identical linker-node bonding chemistry, the Zn−TCPP

DOI: 10.1021/jacs.6b09113
J. Am. Chem. Soc. 2016, 138, 14449−14457

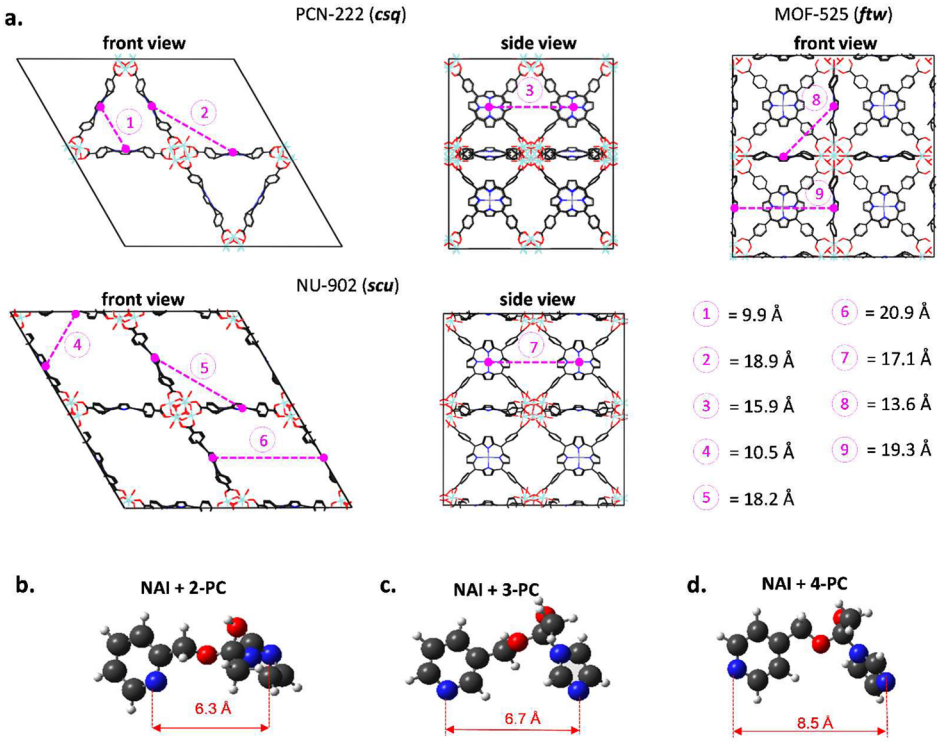

Figure 4. Structural parameters contributing to facilitating the formation of the intermediate. (a) Different center-to-center Zn−Zn distances for different porphyrin pairs in PCN-222 (1−3), NU-902 (4−7), and MOF-525 (8−9). DFT-optimized intermediate-2 configurations corresponding to (b) 2-PC, (c) 3-PC, and (d) 4-PC substrates.

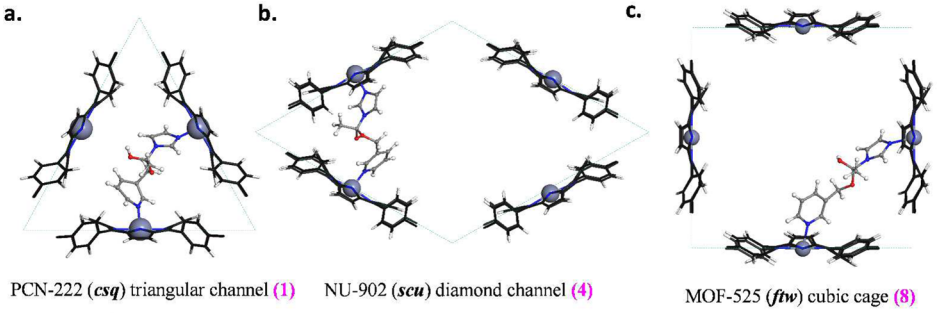

d.

Topology	Pair	Case NAI+2-PC	NAI+3-PC	NAI+4-PC
csq	1	204	242	232
csq	2	2427	1729	1466
csq	3	2065	1542	1358
scu	4	217	203	182
scu	5	2427	1419	1453
scu	6	2831	1558	1515
scu	7	2194	1601	1427
ftw	8	478	261	235
ftw	9	2180	1489	1260

2831 kcal/mol
Strain energy color scale
203 kcal/mol

strain energy = {channel/cage + NAI+PC} − {channel/cage} − {NAI+PC}

Figure 5. (a−c) Molecular mechanics-optimized configurations of intermediate-2 forced to be anchored to porphyrins via N_{NAI}−Zn and N_{PC}−Zn bonds. The configurations correspond to the 3-PC intermediate for the porphyrin pairs of type 1, 4, and 8, with low strain energy. Only selected MOFs atoms are depicted for clarity. Oxygen, red; MOF carbon, black; other carbon, gray; hydrogen, white; nitrogen, blue.

sites in different MOFs should display very similar binding constants for reactants, that is, binding constants that are largely independent of MOF topology. Rate enhancements due to favorable orientation and proximal positioning of NAI and PC by Zn sites, so as to stabilize a transition state (Scheme 1), clearly will be dependent on both the stereochemistry of PC and the topology-imposed positioning of the linkers with respect to each other.

Computational Modeling. We undertook computational modeling studies to qualitatively elucidate how the MOF topology and the identity of the PC regioisomer impact the preconcentration and orientation (i.e., complementary reactant

DOI: 10.1021/jacs.6b09113
J. Am. Chem. Soc. 2016, 138, 14449−14457

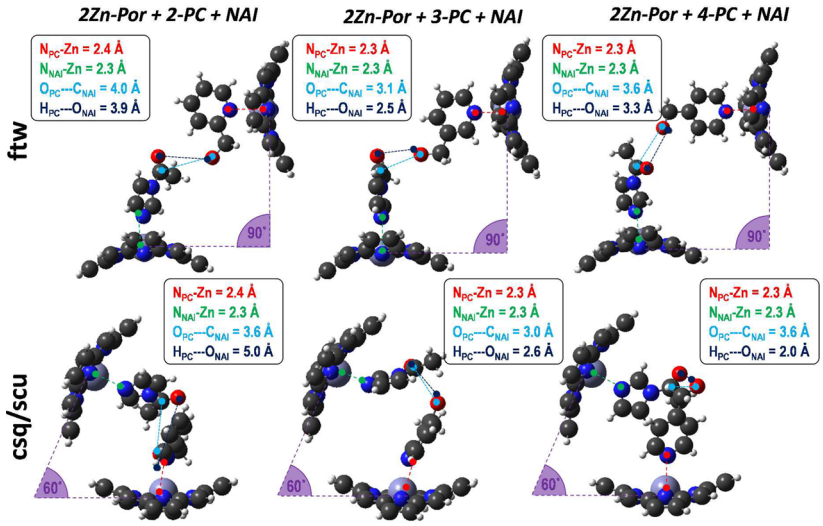

Figure 6. DFT-optimized configurations of MOF-bound reactants. Porphyrin configurations represent different pairs: top row corresponds to type 8 (ftw) pair in Figure 4, while bottom row corresponds to type 1 and 4 (*csq* and *scu*) pairs.

coordination) effects, and whether the computed impact of these effects is consistent with the experimental data.[21] Preconcentration effects are expected to be similar for the three PC regioisomers but to vary across the three MOFs due to differences in the number of Zn−TCPP sites per unit volume of MOF. However, effects related to complementary reactant coordination are more complex to unravel, as they involve pairings of Zn−TCPP sites. Yet not all pairings of Zn−TCPP sites necessarily contribute to facilitating the reaction.

Figure 4a illustrates the possible, symmetrically different pairings of Zn−TCPP sites in PCN-222, NU-902, and MOF-525 with their corresponding Zn−Zn distances. By reasoning that Zn−TCCP sites must be sufficiently close to assist the formation of the transition state in the way illustrated in Scheme 1, we attempted to filter out the pairs that could not possibly contribute to complementary coordination based on a distance criterion. To do this, we focused on intermediate 2, which is a tautomer formed via transfer of the hydroxyl proton to the acyl oxygen (making a more stable "hemiketal"-type intermediate) (Scheme 1). We optimized different conformations of the intermediate-2 for the 2-PC, 3-PC, and 4-PC cases in vacuum using density functional theory (DFT), where those with the largest N_{NAI}−N_{PC} distances are illustrated in Figure 4b−d. We then compared the N_{NAI}−N_{PC} distances in the isolated intermediate 2 with the center-to-center Zn−Zn distances for the different porphyrin pairs. However, the Zn−Zn distances of all porphyrin pairs are moderately to significantly larger than the N_{NAI}−N_{PC} distances in the isolated intermediates (Figure 4), which would rule out all porphyrin pairs. Thus, it follows that the facilitation of the transition state due to complementary coordination may be aided by the "breathing"[22] of the MOF bringing NAI and PC closer together and/or that some level of strain is permissible and necessary to form the transition state (also note that during anchoring N can only come as close to Zn as the N−Zn bond distance allows).

Quantifying the strain energy associated with intermediate-2 can help screen the porphyrin pairs that may be involved in facilitating the transition state formation. Using molecular mechanics (MM) (details in Supporting Information section S4), we evaluated the nine Zn−TCPP pairs shown in Figure 4. In these MM calculations, we "extracted" the relevant Zn−TCPP atoms from the corresponding MOF framework (Figure 5) and anchored the isolated intermediate-2 to the zinc atoms. The atoms of Zn−TCPP remained fixed, whereas the atoms of intermediate-2 were allowed to relax. Zn−N_{NAI} and Zn−N_{PC} bonds were defined (note that MM calculations do not allow bond breaking), and these bonds and all other interatomic interactions were described according to the Universal Force Field.[23] The strain energy was calculated as indicated in Figure 5d. The optimized configurations for the intermediate-2 (3-PC case) for the porphyrin pairs resulting in the lowest strain energies in PCN-222, NU-902, and MOF-525 are summarized in Figure 5a−c. The table in Figure 5d summarizes the calculated strain energy for all cases.

In relative terms, the strain energy for the anchored intermediate (for all PC regioisomers) is much too high in the porphyrin pairs of type 2, 3, 5, 6, 7, and 9 relative to that found in the porphyrin pairs of type 1, 4, and 8. Therefore, we considered that the former set of porphyrin pairs is unlikely to contribute to rate enhancement via complementary binding of reactants, and we focused on the porphyrin pairs of type 1, 4, and 8 (Figure 5a−c). Because the accuracy of MM calculations is limited, we moved on to higher level DFT calculations on the latter set of porphyrin pairs, aiming to gain insight into the suitable MOF-bound reactant (NAI and PC) configurations prior to the formation of the transition state shown in Scheme 1. The goal was to link this information to how the type of PC regioisomer impacts the rate enhancement. To make the DFT calculations affordable, we further reduced the system size relative to that described in Figure 5 by only considering two porphyrin "cores" in our calculations (Figure SI-10). Given the similarities between the type 1 (PCN-222) and type 4 (NU-902) pairs, we only performed DFT calculations on type 1 and 8 (MOF-525) pairs. Only the porphyrin carbon atoms remained fixed during the DFT optimizations.

On the basis of the reaction path postulated in Scheme 1, the initial configurations for these optimizations were defined by placing NAI and PC in perpendicular axial coordination positions to the porphyrins ($N_{NAI/PC}$−Zn = 2.0 Å). We tried to orient the hydroxyl oxygen of PC (O_{PC}) toward the carbonyl carbon of NAI (C_{NAI}), which would facilitate the formation of the transition state, and the hydroxyl hydrogen of PC (H_{PC})

DOI: 10.1021/jacs.6b09113
J. Am. Chem. Soc. 2016, 138, 14449−14457

Table 2. Calculation of the Maximum Number Density of Total and Effective Porphyrin Site Pairs Contributing to Rate Enhancement via Preconcentration and Orientation Effects in MOF-525, NU-902, and PCN-222

MOF	supercell scheme	supercell volume [L]	total Zn−TCPP sites [n]	density of Zn−TCPP [n/L]	max Zn−TCPP in effective pairs [m]	density of Zn−TCPP in effective pair sites [m/L]
MOF-525	2 × 2 × 2	5.7×10^{-17}	24	4.2×10^{17}	24 (8)[a]	4.2×10^{17}
NU-902	2 × 2 × 2	5.2×10^{-17}	16	3.1×10^{17}	16 (4)[a]	3.1×10^{17}
PCN-222	1 × 1 × 2	5.0×10^{-17}	12	2.4×10^{17}	4 (1)[a]	0.8×10^{17}

[a]Numbers in parentheses indicate type of Zn−TCPP pair as shown in Figures 4 and 5.

toward the carbonyl oxygen of NAI (O_{NAI}), which would facilitate the hydrogen transfer going from intermediate-1 to a more stable intermediate-2. The resulting final configurations after optimization are illustrated in Figure 6 (see SI section S6C for additional computational details) along with key distance parameters. In all of the optimized configurations, PC and NAI coordinate with the Zn atoms with $N_{NAI/PC}$−Zn distances around 2.3 Å. In our calculations for the porphyrin pair of type 8 (MOF-525 (***ftw***)), we found the shortest O_{PC}−C_{NAI} and H_{PC}−O_{NAI} distances (3.1 and 2.5 Å, respectively) for the 3-PC system, which seems to be "primed" for the formation of the transition state and subsequent hydrogen transfer generating intermediate 2. The largest O_{PC}−C_{NAI} and H_{PC}−O_{NAI} distances (4.0 and 3.9 Å, respectively) were found for the 2-PC system. In our calculations for the porphyrin pair 1/4 (PCN-222 (***csq***)/NU-902 (***scu***)), we again found the shortest O_{PC}−C_{NAI} distance (3.0 Å) for the 3-PC system, with the H_{PC}−O_{NAI} distance seemingly close enough to facilitate the subsequent hydrogen transfer. In both the 4-PC and the 2-PC systems, the O_{PC}−C_{NAI} distance (3.6 Å) was still seemingly close enough to facilitate formation of the transitions state, but only in the 4-PC case was the H_{PC}−O_{NAI} distance close enough (2.0 Å) to facilitate the subsequent hydrogen transfer.

DISCUSSION

The rate enhancement due to preconcentration effects arises when NAI and PC diffuse into the MOF and bind to the porphyrins via N_{NAI}−Zn and N_{PC}−Zn interactions. The binding populates the porphyrins with NAI and PC, resulting in a large number of molecules confined in a small volume, making it more probable for them to encounter each other and react. Thus, more prominent preconcentration effects are expected with more porphyrin sites per volume of MOF. The number density of Zn−TCPPs in each MOF follows the order PCN-222 < NU-902 < MOF-525 as listed in Table 2 and calculated from the supercells in Figure 4.

Assuming that the rate enhancement due to preconcentration tracks linearly with the number density of Zn−TCCPs, PCN-222 (***csq***) is expected to present the lowest rate enhancement, consistent with the data presented in Table 1 (or Figure 7d). Because the differences in DFT-calculated binding energies among the PC reactants are negligible (<2 kJ/mol), no differences in rate enhancement due to preconcentration are expected across the three PC regioisomers for any given MOF (Figure 7a). However, the reaction rates in a given MOF are different for 2-PC, 3-PC, and 4-PC (Figure 7d), and the relative rates for a given PC regioisomer across the MOFs (Figure 7d) are different from what would be expected if only preconcentration effects (Figure 7a) were responsible. Therefore, we believe these differences are due to orientation effects in the different MOF topologies. With our calculations (MM and DFT), we identified that only the porphyrin pairs of type 1, 4, and 8 in PCN-222 (***csq***), NU-902 (***scu***), and MOF-525 (***ftw***),

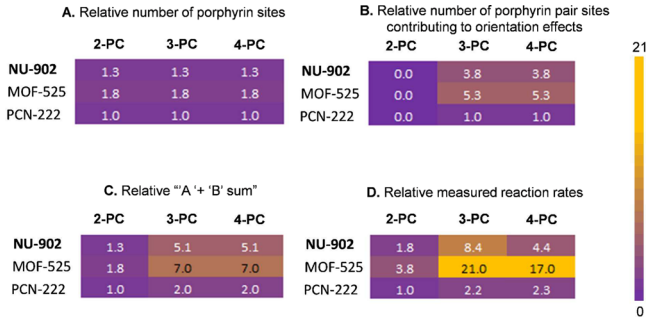

Figure 7. Relative values of number of porphyrin sites (a), porphyrin pairs linked to orientation effects (b), porphyrin sites plus porphyrin pairs (c), and measured reaction rates (d). Color scale bar applies to all four tables.

respectively, can result in the complementary reactant binding necessary to engender such orientation effects. One cubic cage of MOF-525 (***ftw***), which is lined by six Zn−TCCPs, provides a maximum of three porphyrin pairs of type 8 at any given time for a total of 24 pairs in the supercell shown in Figure 4a. One basic diamond channel section of NU-902 (***scu***), which is lined by four Zn−TCCPs, provides a maximum of two porphyrin pairs of type 4 at any given time for a total of 16 pairs in the supercell shown in Figure 4a. Finally, one triangular channel section of PCN-222 (***csq***) is lined by three Zn−TCCPs and can only provide a maximum of one porphyrin pair of type 1 at any given time for a total of four pairs in the supercell shown in Figure 4a (note that the hexagonal channels of PCN-222 only contribute to preconcentration effects). With these considerations, the estimated maximum number of porphyrin pairs that contribute to orientation effects follows the order PCN-222 < NU-902 < MOF-525 as listed in Table 2 and calculated from the supercells in Figure 4. On the basis of our DFT optimizations for the "MOF-bound" NAI and PC, it is unlikely that orientation effects contribute significantly to rate enhancement in the 2-PC systems (due to the distances between atoms involved in the transition state and hydrogen transfer); hence we set the density of porphyrin pairs contributing to orientation effects as zero (Figure 7b).

Figure 7a shows the relative number of porphyrin sites accessible for each regioisomer in each MOF, which would be similar to the relative reaction rates for each regioisomer in the different MOFs if preconcentration were the only contributing factor. Figure 7b shows the relative number of porphyrin pairs accessible for each regiosiomer reaction case, which would be similar to the relative reaction rates for each regioisomer in different MOFs if orientation effects were the only factor contributing to rate enhancement. A very simple, preliminary way to qualitatively account for the combination of preconcentration and orientation effects is to add up the two relative contributions as shown in Figure 7c. Comparison of these combined relative contributions (Figure 7c) with relative

DOI: 10.1021/jacs.6b09113
J. Am. Chem. Soc. 2016, 138, 14449−14457

experimental rates (Figure 7d) reveals that the combination of the two effects (represented by the number of porphyrin sites and effective porphyrin pairs) largely accounts for the trends in reaction rates experimentally measured for 2-PC, 3-PC, and 4-PC in NU-902, MOF-525, and PCN-222. The above provides a rationale for the sizable sensitivity of MOF catalytic activity to MOF topology. However, note that our analysis does not account for factors including, but not limited to, the (i) probability for the population to consist of NAI and PC reactants coordinated to adjacent sites corresponding to an effective Zn−TCPP pair, (ii) relative diffusion rates of the reactants, (iii) relative dissociation constants of the products, and (iv) energetics of transition states.

CONCLUSIONS

We find that MOFs featuring Lewis acidic (porphinato)zinc(II) species as linkers, including the newly introduced MOF NU-902, are capable of catalyzing the transfer of an acyl group from NAI to 2-PC, 3-PC, and 4-PC. NU-902 features diamond channels and is based on the ***scu*** topology. PCN-222 (***csu***), MOF-525 (***ftw***), and NU-902 define a series of MOFs that present nominally chemically identical catalytic sites (i.e., under-coordinated, Lewis acidic, Zn(II) ions). They differ from each other, however, in terms of the number of sites they present and in how they organize pairs of such sites spatially. All three MOFs display catalytic activity for acyl transfer to all three regio-isomers. The degree of catalysis, however, is significantly dependent on both the identity of the PC regio-isomer and the identity of the MOF. Indeed, relative rates differ by as much as 20-fold.

Baseline catalytic activity is attributable to preconcentration of either or both reactants via axial coordination by Zn(II), and to zinc-based Lewis-acid activation of *N*-acetylimidazole. Differences in catalytic activity as a function of MOF topology and as a function of PC regio-isomer identity can be qualitatively understood in terms of the ability of pairs of Zn−TCCP sites within each MOF to position the acyl-group donor and acceptor species at suitable distances and relative orientations to facilitate transition-state formation.

In summary, this work demonstrates how a high density of catalytic sites combined with specific spatial orientations of those sites can engender a supramolecular catalytic machine that works concertedly to facilitate the formation of relevant transition states and, in turn, enhance reaction rates. The extant diversity of MOF topologies suggests that these porous frameworks will prove to be useful organizational structures for a rich variety of multisite-catalyzed chemical reactions.

ASSOCIATED CONTENT

Supporting Information

The Supporting Information is available free of charge on the ACS Publications website at DOI: 10.1021/jacs.6b09113.

Procedure, characterization (NMR, DRIFTS), SEM-EDS, N_2 sorption data, and computational details (PDF)
X-ray crystallographic data (CIF)

AUTHOR INFORMATION

Corresponding Authors

*pderia@siu.edu
*snurr@northwestern.edu
*j-hupp@northwestern.edu
*o-farha@northwestern.edu

Present Address

[⊥]Department of Chemical and Biological Engineering, Colorado School of Mines, Golden, Colorado 80401, United States.

Author Contributions

[#]P.D. and D.A.G.-G. contributed equally.

Notes

The authors declare no competing financial interest.

ACKNOWLEDGMENTS

We gratefully acknowledge funding from the National Science Foundation (grant DMR-1334928). DFT calculations were made possible thanks to NERSC computational resources. PXRD data were collected at the J.B. Cohen X-ray Diffraction Facility (supported by the NSF MRSEC program DMR-1121262) of the Materials Research Center of Northwestern University. FT-IR data were collected in the NUANCE Center (supported by the NSF-NSEC and -MRSEC programs, the Keck Foundation, the State of Illinois, and Northwestern University) at Northwestern University.

REFERENCES

(1) (a) Férey, G. *Chem. Soc. Rev.* **2008**, *37*, 191. (b) Furukawa, H.; Cordova, K. E.; O'Keeffe, M.; Yaghi, O. M. *Science* **2013**, *341*, 1230444. (c) Horike, S.; Shimomura, S.; Kitagawa, S. *Nat. Chem.* **2009**, *1*, 695. (d) Farha, O. K.; Hupp, J. T. *Acc. Chem. Res.* **2010**, *43*, 1166.

(2) (a) Eddaoudi, M.; Kim, J.; Rosi, N.; Vodak, D.; Wachter, J.; O'Keeffe, M.; Yaghi, O. M. *Science* **2002**, *295*, 469. (b) Yaghi, O. M.; O'Keeffe, M.; Ockwig, N. W.; Chae, H. K.; Eddaoudi, M.; Kim, J. *Nature* **2003**, *423*, 705. (c) Férey, G. *Chem. Soc. Rev.* **2008**, *37*, 191. (d) Kitagawa, S.; Kitaura, R.; Noro, S.-i. *Angew. Chem., Int. Ed.* **2004**, *43*, 2334. (e) Deng, H.; Doonan, C. J.; Furukawa, H.; Ferreira, R. B.; Towne, J.; Knobler, C. B.; Wang, B.; Yaghi, O. M. *Science* **2010**, *327*, 846. (f) O'Keeffe, M.; Yaghi, O. M. *Chem. Rev.* **2012**, *112*, 675. (g) Guillerm, V.; Kim, D.; Eubank, J. F.; Luebke, R.; Liu, X.; Adil, K.; Lah, M. S.; Eddaoudi, M. *Chem. Soc. Rev.* **2014**, *43*, 6141. (h) Wilmer, C. E.; Leaf, M.; Lee, C. Y.; Farha, O. K.; Hauser, B. G.; Hupp, J. T.; Snurr, R. Q. *Nat. Chem.* **2011**, *4*, 83.

(3) (a) Lee, J.; Farha, O. K.; Roberts, J.; Scheidt, K. A.; Nguyen, S. T.; Hupp, J. T. *Chem. Soc. Rev.* **2009**, *38*, 1450. (b) Ma, L.; Abney, C.; Lin, W. *Chem. Soc. Rev.* **2009**, *38*, 1248. (c) Liu, J.; Chen, L.; Cui, H.; Zhang, J.; Zhang, L.; Su, C.-Y. *Chem. Soc. Rev.* **2014**, *43*, 6011. (d) Yoon, M.; Srirambalaji, R.; Kim, K. *Chem. Rev.* **2012**, *112*, 1196.

(4) Karagiaridi, O.; Lalonde, M. B.; Bury, W.; Sarjeant, A. A.; Farha, O. K.; Hupp, J. T. *J. Am. Chem. Soc.* **2012**, *134*, 18790.

(5) (a) Feng, D.; Gu, Z.-Y.; Li, J.-R.; Jiang, H.-L.; Wei, Z.; Zhou, H.-C. *Angew. Chem., Int. Ed.* **2012**, *51*, 10307. (b) Jiang, H.-L.; Feng, D.; Wang, K.; Gu, Z.-Y.; Wei, Z.; Chen, Y.-P.; Zhou, H.-C. *J. Am. Chem. Soc.* **2013**, *135*, 13934. (c) Nakagaki, S.; Ferreira, G. K. B.; Ucoski, G. M.; Dias de Freitas Castro, K. A. *Molecules* **2013**, *18*, 7279.

(6) (a) Beyzavi, M. H.; Vermeulen, N. A.; Howarth, A. J.; Tussupbayev, S.; League, A. B.; Schweitzer, N. M.; Gallagher, J. R.; Platero-Prats, A. E.; Hafezi, N.; Sarjeant, A. A.; Miller, J. T.; Chapman, K. W.; Stoddart, J. F.; Cramer, C. J.; Hupp, J. T.; Farha, O. K. *J. Am. Chem. Soc.* **2015**, *137*, 13624. (b) Srirambalaji, R.; Hong, S.; Natarajan, R.; Yoon, M.; Hota, R.; Kim, Y.; Ko, Y. H.; Kim, K. *Chem. Commun.* **2012**, *48*, 11650. (c) Song, F.; Wang, C.; Lin, W. *Chem. Commun.* **2011**, *47*, 8256. (d) Manna, K.; Zhang, T.; Greene, F. X.; Lin, W. *J. Am. Chem. Soc.* **2015**, *137*, 2665.

(7) Gómez-Gualdron, D. A.; Gutov, O. V.; Krungleviciute, V.; Borah, B.; Mondloch, J. E.; Hupp, J. T.; Yildirim, T.; Farha, O. K.; Snurr, R. Q. *Chem. Mater.* **2014**, *26*, 5632.

(8) Katz, M. J.; Moon, S.-Y.; Mondloch, J. E.; Beyzavi, M. H.; Stephenson, C. J.; Hupp, J. T.; Farha, O. K. *Chemical Science* **2015**, *6*, 2286.

(9) (a) Cavka, J. H.; Jakobsen, S.; Olsbye, U.; Guillou, N.; Lamberti, C.; Bordiga, S.; Lillerud, K. P. *J. Am. Chem. Soc.* **2008**, *130*, 13850.

DOI: 10.1021/jacs.6b09113
J. Am. Chem. Soc. 2016, 138, 14449−14457

(b) Mondloch, J. E.; Katz, M. J.; Planas, N.; Semrouni, D.; Gagliardi, L.; Hupp, J. T.; Farha, O. K. *Chem. Commun.* **2014**, *50*, 8944. (c) Wu, H.; Chua, Y. S.; Krungleviciute, V.; Tyagi, M.; Chen, P.; Yildirim, T.; Zhou, W. *J. Am. Chem. Soc.* **2013**, *135*, 10525. (d) Wu, H.; Yildirim, T.; Zhou, W. *J. Phys. Chem. Lett.* **2013**, *4*, 925.

(10) Feng, D.; Liu, T.-F.; Su, J.; Bosch, M.; Wei, Z.; Wan, W.; Chen, Y.-P.; Wang, X.; Wang, K.; Lian, X.; Gu, Z.-Y.; Park, J.; Yuan, D.; Zou, X.; Zhou, H.-C. *Nat. Commun.* **2015**, *6*, 5979.

(11) (a) Chen, Y.; Hoang, T.; Ma, S. *Inorg. Chem.* **2012**, *51*, 12600. (b) Mondloch, J. E.; Bury, W.; Fairen-Jimenez, D.; Kwon, S.; DeMarco, E. J.; Weston, M. H.; Sarjeant, A. A.; Nguyen, S. T.; Stair, P. C.; Snurr, R. Q.; Farha, O. K.; Hupp, J. T. *J. Am. Chem. Soc.* **2013**, *135*, 10294. (c) Morris, W.; Volosskiy, B.; Demir, S.; Gándara, F.; McGrier, P. L.; Furukawa, H.; Cascio, D.; Stoddart, J. F.; Yaghi, O. M. *Inorg. Chem.* **2012**, *51*, 6443. (d) Vermoortele, F.; Vandichel, M.; Van de Voorde, B.; Ameloot, R.; Waroquier, M.; Van Speybroeck, V.; De Vos, D. E. *Angew. Chem., Int. Ed.* **2012**, *51*, 4887. (e) Feng, D.; Gu, Z.-Y.; Chen, Y.-P.; Park, J.; Wei, Z.; Sun, Y.; Bosch, M.; Yuan, S.; Zhou, H.-C. *J. Am. Chem. Soc.* **2014**, *136*, 17714. (f) Pullen, S.; Fei, H.; Orthaber, A.; Cohen, S. M.; Ott, S. *J. Am. Chem. Soc.* **2013**, *135*, 16997. (g) Fei, H.; Pullen, S.; Wagner, A.; Ott, S.; Cohen, S. M. *Chem. Commun.* **2015**, *51*, 66. (h) Kalidindi, S. B.; Nayak, S.; Briggs, M. E.; Jansat, S.; Katsoulidis, A. P.; Miller, G. J.; Warren, J. E.; Antypov, D.; Corà, F.; Slater, B.; Prestly, M. R.; Mart-Gastaldo, C.; Rosseinsky, M. J. *Angew. Chem., Int. Ed.* **2015**, *54*, 221. (i) deKrafft, K. E.; Boyle, W. S.; Burk, L. M.; Zhou, O. Z.; Lin, W. *J. Mater. Chem.* **2012**, *22*, 18139. (j) Tulig, K.; Walton, K. S. *RSC Adv.* **2014**, *4*, 51080. (k) Nunes, P.; Gomes, A. C.; Pillinger, M.; Gonçalves, I. S.; Abrantes, M. *Microporous Mesoporous Mater.* **2015**, *208*, 21. (l) Feng, D.; Chung, W.-C.; Wei, Z.; Gu, Z.-Y.; Jiang, H.-L.; Chen, Y.-P.; Darensbourg, D. J.; Zhou, H.-C. *J. Am. Chem. Soc.* **2013**, *135*, 17105. (m) Mondloch, J. E.; Katz, M. J.; Isley, W. C., III; Ghosh, P.; Liao, P.; Bury, W.; Wagner, G. W.; Halls, M. G.; DeCoste, J. B.; Peterson, G. W.; Snurr, R. Q.; Cramer, C. J.; Hupp, J. T.; Farha, O. K. *Nat. Mater.* **2015**, *14*, 512.

(12) (a) Farha, O. K.; Shultz, A. M.; Sarjeant, A. A.; Nguyen, S. T.; Hupp, J. T. *J. Am. Chem. Soc.* **2011**, *133*, 5652. (b) Shultz, A. M.; Farha, O. K.; Hupp, J. T.; Nguyen, S. T. *J. Am. Chem. Soc.* **2009**, *131*, 4204. (c) Gao, W.-Y.; Chrzanowski, M.; Ma, S. *Chem. Soc. Rev.* **2014**, *43*, 5841.

(13) Mackay, L. G.; Wylie, R. S.; Sanders, J. K. M. *J. Am. Chem. Soc.* **1994**, *116*, 3141.

(14) Rouquerol, J.; Llewellyn, P.; Rouquerol, F. *Stud. Surf. Sci. Catal.* **2007**, *160*, 49.

(15) Gómez-Gualdrón, D. A.; Moghadam, P. Z.; Hupp, J. T.; Farha, O. K.; Snurr, R. Q. *J. Am. Chem. Soc.* **2016**, *138*, 215.

(16) (a) Hod, I.; Sampson, M. D.; Deria, P.; Kubiak, C. P.; Farha, O. K.; Hupp, J. T. *ACS Catal.* **2015**, *5*, 6302. (b) Kung, C.-W.; Chang, T.-H.; Chou, L.-Y.; Hupp, J. T.; Farha, O. K.; Ho, K.-C. *Chem. Commun.* **2015**, *51*, 2414.

(17) (a) Deria, P.; Bury, W.; Hod, I.; Kung, C.-W.; Karagiaridi, O.; Hupp, J. T.; Farha, O. K. *Inorg. Chem.* **2015**, *54*, 2185. (b) Deria, P.; Bury, W.; Hupp, J. T.; Farha, O. K. *Chem. Commun.* **2014**, *50*, 1965. (c) Deria, P.; Mondloch, J. E.; Karagiaridi, O.; Bury, W.; Farha, O. K.; Hupp, J. T. *Chem. Soc. Rev.* **2014**, *43*, 5896. (d) Deria, P.; Mondloch, J. E.; Tylianakis, E.; Ghosh, P.; Bury, W.; Snurr, R. Q.; Hupp, J. T.; Farha, O. K. *J. Am. Chem. Soc.* **2013**, *135*, 16801.

(18) (a) Valenzano, L.; Civalleri, B.; Chavan, S.; Bordiga, S.; Nilsen, M. H.; Jakobsen, S.; Lillerud, K. P.; Lamberti, C. *Chem. Mater.* **2011**, *23*, 1700. (b) Oliveri, C. G.; Gianneschi, N. C.; Nguyen, S. T.; Mirkin, C. A.; Stern, C. L.; Wawrzak, Z.; Pink, M. *J. Am. Chem. Soc.* **2006**, *128*, 16286.

(19) Note also that the relative intensities of the intense peaks appearing at 2θ values of 4.8 and 7.1 for NU-902 are consistent with the model for NU-902 but not for PCN-223; see SI section S2.

(20) A control experiment with a nonmetallated MOF was found to be extremely slow, only ~5% turnover even after 27 h with an initial rate of ~0.01 mM/h.

(21) Roy, S.; George, C. B.; Ratner, M. A. *J. Phys. Chem. C* **2012**, *116*, 23494.

(22) Deria, P.; Gómez-Gualdrón, D. A.; Bury, W.; Schaef, H. T.; Wang, T. C.; Thallapally, P. K.; Sarjeant, A. A.; Snurr, R. Q.; Hupp, J. T.; Farha, O. K. *J. Am. Chem. Soc.* **2015**, *137*, 13183.

(23) Rappé, A. K.; Casewit, C. J.; Colwell, K. S.; Goddard, W. A.; Skiff, W. M. *J. Am. Chem. Soc.* **1992**, *114*, 10024.

DOI: 10.1021/jacs.6b09113
J. Am. Chem. Soc. 2016, 138, 14449−14457